ACS APPLIED MATERIALS & INTERFACES

Research Article

www.acsami.org

Strong and Moldable Cellulose Magnets with High Ferrite Nanoparticle Content

Sylvain Galland,[†,‡,∥] Richard L. Andersson,[‡] Valter Ström,[§] Richard T. Olsson,*[,†,‡] and Lars A. Berglund*[,†,‡]

[†]KTH − Royal Institute of Technology, Fibre and Polymer Technology, Wallenberg Wood Science Center, Teknikringen 56, 100 44 Stockholm, Sweden

[‡]KTH − Royal Institute of Technology, School of Chemical Science and Engineering, Fibre and Polymer Technology, Teknikringen 56, 100 44 Stockholm, Sweden

[§]Department of Materials Science and Engineering, KTH − Royal Institute of Technology, Brinellvägen 23, 100 44 Stockholm, Sweden

ABSTRACT: A major limitation in the development of highly functional hybrid nanocomposites is brittleness and low tensile strength at high inorganic nanoparticle content. Herein, cellulose nanofibers were extracted from wood and individually decorated with cobalt-ferrite nanoparticles and then for the first time molded at low temperature (<120 °C) into magnetic nanocomposites with up to 93 wt % inorganic content. The material structure was characterized by TEM and FE-SEM and mechanically tested as compression molded samples. The obtained porous magnetic sheets were further impregnated with a thermosetting epoxy resin, which improved the load-bearing functions of ferrite and cellulose material. A nanocomposite with 70 wt % ferrite, 20 wt % cellulose nanofibers, and 10 wt % epoxy showed a modulus of 12.6 GPa, a tensile strength of 97 MPa, and a strain at failure of ca. 4%. Magnetic characterization was performed in a vibrating sample magnetometer, which showed that the coercivity was unaffected and that the saturation magnetization was in proportion with the ferrite content. The used ferrite, $CoFe_2O_4$, is a magnetically hard material, demonstrated by that the composite material behaved as a traditional permanent magnet. The presented processing route is easily adaptable to prepare millimeter-thick and moldable magnetic objects. This suggests that the processing method has the potential to be scaled-up for industrial use for the preparation of a new subcategory of magnetic, low-cost, and moldable objects based on cellulose nanofibers.

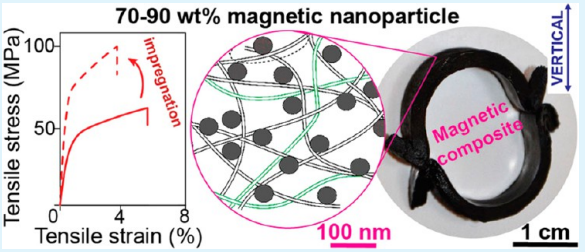

KEYWORDS: *cellulose nanofiber, ferrite nanoparticle, nanocomposite, compression-molding, mechanical properties, magnetic composite, epoxy, material processing*

INTRODUCTION

Nanometer confinement, structural or geometrical anisotropy, and large surface to volume ratio are characteristics of nanoparticles, which allow their properties to be very different from the bulk materials.[1−3] Polymer nanocomposites based on inorganic nanoparticles therefore make it possible to explore novel combinations of material properties and functionalities,[4,5] including improved dielectric, optical, conductive, mechanical, or magnetic properties. Some of the most widely studied nanoparticles include silica (SiO_2),[6] titania (TiO_2),[7] carbon,[8] clay,[9] and ferrites.[10,11] So far, attempts to combine the favorable properties of both polymeric and inorganic nanoparticles[12] have mostly relied on relatively low particle content (up to ∼10 wt %) to mechanically reinforce the polymer.[13−16] For high nanoparticle content (>10 vol %), the mechanical properties are usually compromised because of poor polymer/nanoparticle compatibility leading to particle aggregation.[17,18] A common approach is then to use nanoparticles with surface modification to improve compatibility with the polymer matrix or introduction of repulsive forces between nanoparticles for better dispersion.[12,19,20] These strategies are still problematic for high nanoparticle contents. The classical mixing routes also face the difficulty of high viscosity of the polymer/nanoparticle blend, and this limits the processing possibilities.[21]

The obvious advantage of high filler content is that the functionality generally scales strongly with nanoparticle content, e.g. catalytic, optical or magnetic materials, in combination with good mechanical properties. A number of approaches have therefore been proposed to prepare nanocomposites with high filler contents. In situ surface initiated polymerization onto inorganic nanoparticles can be used, where the amount of polymer matrix is controlled by the degree of polymerization and grafting density at the particle surface.[12] The nanocomposite is then obtained by evaporating the

Received: September 9, 2014
Accepted: October 20, 2014
Published: October 20, 2014

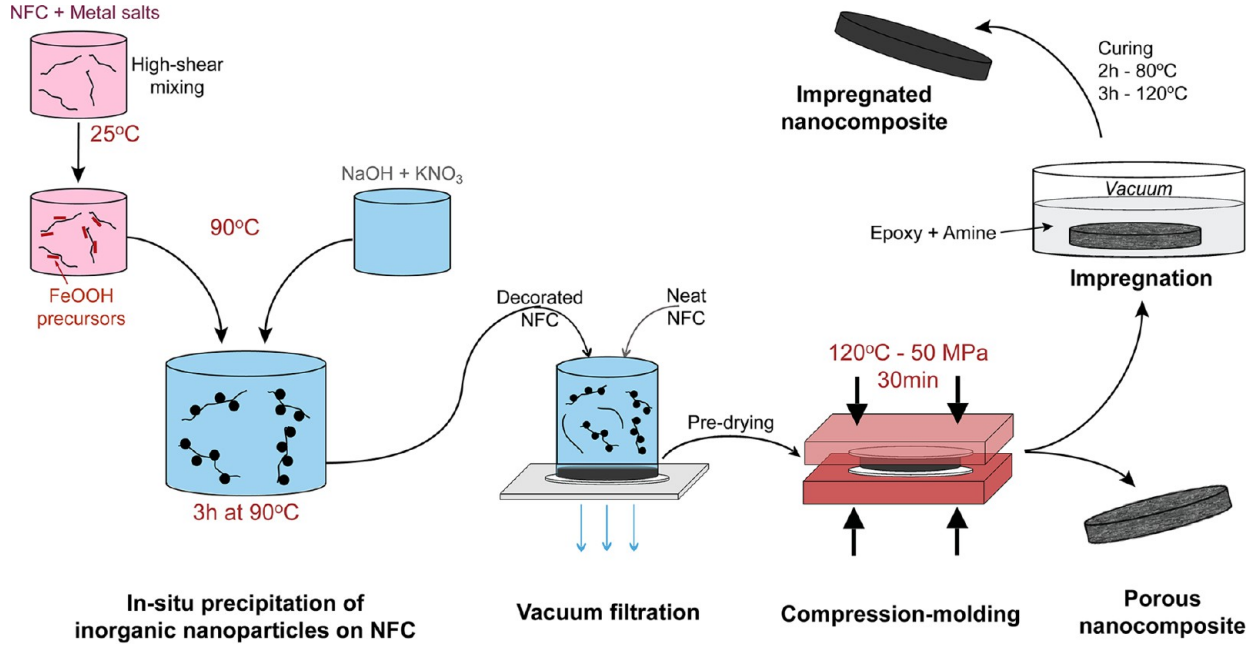

Figure 1. Low temperature processing route toward high inorganic content compression-molded magnetic nanocomposites.

solvent, bringing the coated nanoparticles in close contact. Zhanhu et al.[22] reported materials with up to 30 vol % (65 wt %) of iron oxide in polyurethane. Another method is to adsorb the polymer onto the nanoparticle surface. To reach high inorganic content the excess nonadsorbed polymer can be washed away, and the solvent evaporated or filtered to obtain the nanocomposite.[23] The technique was used to prepare nacre-mimetic nanocomposites based on montmorillonite clay platelets coated with a polymer. The inorganic content was as high as 50 vol %.[23−25] Layer-by-layer adsorption techniques have also been used.[26,27] However, with some exception these methods are generally limited to small samples, and the processes are hardly adaptable to large-scale industrial production.

In this article, we report cellulose nanocomposite magnets with inorganic nanoparticle content up to 93 wt %. They are based on cellulose nanofibers (NFC) decorated by magnetic nanoparticles, which can be diluted by neat NFC to any desirable magnetic nanoparticle content. The dispersion of the inorganic phase is retained. This allows for magnetic cellulose nanocomposites that are capable of magnetically supporting more than their own weight, i.e. as traditional permanent magnets, with the added advantage of lightweight materials (due to the low density). The cellulose magnets were compression-molded at 50 MPa and 120 °C into solid blocks. Previously, several works have reported mechanical properties up to 60 MPa strength at ferrite nanoparticle contents in the range 20−25 wt %, i.e. 5−7 vol %.[28−30] We demonstrate that compression-molding of magnetic particle decorated cellulose fibrils is a method to obtain equivalent mechanical properties for composites containing 8 times more inorganic nanoparticles−with preserved, and predictable magnetic characteristics. In addition; the obtained nanoporous structure of the obtained hybrid NFC/nanoparticle composites allowed for impregnation with an epoxy resin, which further strengthened the already tough and condensed nanofibril networks. Finally, we illustrate the scale-up potential by preparing millimeter thick magnetic plates and components by compression-molding stacks of wet nanocomposite sheets. The presented "master-batch" approach thus appears technically feasible to manufacture nanostructured cellulose magnet components of complex shape on large industrial scale. It also opens for more efficient preparation and handling of highly functional cellulose nanofibers in a similar fashion as "mater−batch" techniques are used in polymer engineering processing.

EXPERIMENTAL SECTION

Precipitation of $CoFe_2O_4$ Nanoparticles onto Cellulose Nanofibrils (NFC). Cellulose nanofibrils were extracted from sulfite pulp (Nordic Paper, Sweden) with hemicelluloses and lignin contents of 13.8 and 0.7 wt % and a cellulose degree of polymerization of 1200. Compared with conventional highly fibrillated pulp by disk refining, the following pretreatment lowers energy requirements for disintegration. Furthermore, small diameter nanofibers provide better mechanical properties than fibrillated pulp and more homogeneous distribution of inorganic particles. The NFC extraction was made via enzymatic pretreatment for 2 h at 50 °C in a 0.25 vol % aqueous solution of endoglucanase enzyme Novozyme 476 (0.1 mL enzyme/40 g dry content cellulose).[31] The treatment was followed by 8 passes at 1200 bar pressure through a microfluidizer (M-110EH, Microfluidics Ind., USA) to liberate the cellulose nanofibrils (average nanofibril width: 10 nm[32,33]). A suspension with ca. 2 wt % nanofibril content was obtained. The suspension was diluted to 0.30 wt % prior to in situ $CoFe_2O_4$ nanoparticle precipitation along the fibrils.[34] Briefly, reagent grade iron(II) sulfate heptahydrate and cobalt(II) chloride hexahydrate (Sigma-Aldrich, Sweden) were added to the suspension under high-shear mixing at 13000 rpm (Ultra-Turrax D125, IKA, Germany). The molar ratio of cobalt to iron was 1:2. Sodium hydroxide and potassium nitrate (reagent grade, Sigma-Aldrich) were dissolved in water separately. The ratio $[Me^{2+}]/[OH^-]$ and $[Me^{2+}]/[KNO_3]$ were 1:2 and 1:3, respectively. All solutions were heated to 90 °C for 40 min under mechanical stirring, and the alkaline solution was added into the metal ion cellulose suspension. The reaction time was 3 h at 90 °C to ensure complete conversion of the metal oxide-hydroxide complexes to the spinel ferrite phase along the fibrils. The processing route is illustrated in Figure 1. The decorated nanofibrils were rinsed 4 times with deionized water. The amounts of metal salts were calculated to yield hybrid cellulose nanofibrils with 96.5 wt % (90 vol %) of $CoFe_2O_4$, corresponding to salt

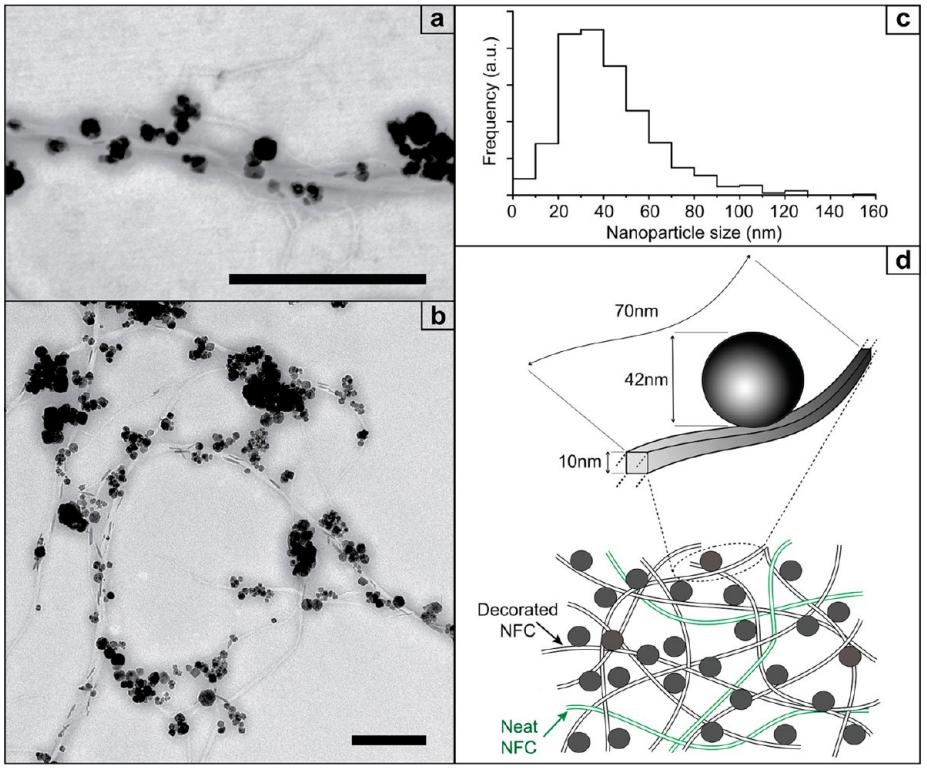

Figure 2. a,b: TEM micrographs of cellulose nanofibrils decorated with 96.5 wt % $CoFe_2O_4$ nanoparticles (scale bars: 500 nm) showing that all particles are associated with fibers; **c**: Particle size distribution from TEM image analysis; **d**: Illustration of a representative segment of decorated NFC and of the final hybrid network including some neat NFC.

concentrations of 579 mM in Fe^{2+} and 290 mM in Co^{2+}. The yield was confirmed accurate from TG measurements (Figure 7 and Table 2).

Preparation of High Magnetic Particle Content Nanocomposites by Compression-Molding. The magnetically decorated NFC was mixed (i.e., diluted) with untreated NFC (Figure 1) to reach final nanoparticle contents of 77, 83, 89, and 93 wt % (50, 60, 70, and 80 vol % with respect to amount of solid material) in the nanocomposite. High-shear mixing (13000 rpm) was subsequently performed for 5 min combined with vacuum degassing for 10 min before the suspensions were vacuum filtered through a 0.65 μm pore-size filter membrane (DVPP, Millipore, USA). No apparent amount of dry residue was found in the filtrate, indicating insignificant loss of material during filtration. The filtrate was completely transparent.

The obtained hydrogel "cake" consisted of 60−70 wt % of water, which was reduced to 40−50 wt % by predrying in an oven at 60 °C for 15 min. The predrying was required to prevent flowing under the high-pressure molding. The compression-molding was performed for 30 min at 120 °C under 50 MPa pressure to ensure complete drying of the material and minimize the porosity (Figure 1). Two 0.1 μm pore-size membranes (VVPP, Millipore, USA) were used to blot each side of the "cake" during hot pressing to allow for steam evacuation while preserving a smooth compressed sheet surface. Sheets with 120−150 μm thicknesses were obtained with a porosity of ca. 30−35%, as determined from density measurements (see below). Multilayer composite plates were prepared by stacking 10 wet sheets from the filtration step, yielding 1.2 mm thick magnetic plates.

Epoxy Resin Impregnation of Magnetic Cellulose Sheets. The dry porous magnetic cellulose sheets were impregnated with monomeric diglycidyl ether of bisphenol A (DGEBA) epoxy from Tokyo Chemical Industry mixed with polyetheramine (60/40 wt %) (Jeffamine D-400, Huntsman, USA). The resin was heated to 60 °C before the sheets were immersed and placed in a vacuum chamber for 5 min to promote penetration of the resin (Figure 1). Excess resin was wiped from the material's surface. The curing was performed in an oven for 2 h at 80 °C followed by a post curing step at 120 °C for 3 h. A previous study confirms favorable properties of this NFC/epoxy composite.[35]

Transmission Electron Microscopy (TEM) of Decorated NFC. A water drop with ca. 0.01 wt % decorated nanofibrils was deposited on the top of a TEM grid (400 mesh, Ultrathin carbon film, Ted Pella, USA). It was removed after 1 min by blotting with filter paper. The grid was observed in a transmission electron microscope (TEM, Hitachi HT-7700, Japan).

Structural Characterization of Nanocomposites. Fracture surface cross sections of the sheets and plates were observed in a field emission scanning electron microscope (FE-SEM, Hitachi S-4300, Japan) after 20 s sputtering (ca. 5 nm gold−palladium conductive layer) with a Cressington 208HR, UK. The densities of the nanocomposites were measured by gravimetry and volumetry, and the porosities were estimated based on known densities of the components ($CoFe_2O_4$ nanoparticles:[36] 4.9 g/cm^3; NFC:[37] 1.45 g/cm^3; epoxy: 1.08 g/cm^3).

Mechanical Testing. The nanocomposite sheets were tested in tension, whereas the multilayer plates were tested by three-point bending. All tests were carried out on a universal testing system (Instron 5944, UK) equipped with a 500N load-cell. For tensile testing, specimens were strips 5−6 mm wide, 120−150 μm thick. The specimens were placed in the test room, conditioned at 25 °C and 50% RH, at least 48 h before testing. In order to accurately determine strains of the comparably small specimens, the gauge length was set to 20 mm and the cross-head displacement to 10%/min. The strain values were recorded by 2D digital speckle photography and image correlation (Limess Vic-2D system, Correlated Solutions Inc., USA), where the Young's modulus was calculated as the slope at low strain values. For the bending tests, 7−8 mm bars of the plates were used (thickness 1.2 mm). The span length was set to 20 mm, and the cross-head displacement was 1 mm/min.

Magnetic Properties. Magnetic characterization was performed at room temperature in a vibrating sample magnetometer (VSM, Oxford Instruments, UK). The applied magnetic field strength was varied in

the range ±500 kA/m, and the measurements were performed on thin strips (5 × 2 mm) from the 120 μm thick sheets.

Thermogravimetric Analysis (TGA). Samples of ca. 10 mg were analyzed by thermogravimetry (Mettler-Toledo TGA/SDTA851, Switzerland) under 50 mL/min O_2 flow at a heating rate of 10 °C/min. The samples were held for 10 min at 100 °C to remove loosely bound water and another 10 min at 120 °C to eliminate all water. The mass at this point was taken as the dry mass of the samples. The analysis was completed by a third heating (10 °C/min) to 550 °C to degrade all organic matter. The residual weight after this heating was used for the calculation of the inorganic (i.e., $CoFe_2O_4$) concentration.

Dynamic Thermomechanical Analysis (DMTA). DMTA was performed on a Q800 DMA analyzer (TA Instruments, USA) in tension mode at a frequency of 1 Hz and amplitude of 10 μm. The temperature was ramped from 25 to 220 °C with a rate of 5 °C/min. Specimens were 4−5 mm wide strips (ca. 120 μm thick), and the gauge lengths was 6−8 mm. The storage modulus (E') data were vertically adjusted to the corresponding tensile modulus values at 25 °C. Relative changes in E' with temperature were therefore analyzed, rather than absolute values for storage modulus.

RESULTS AND DISCUSSION

NFC Nanofibers Decorated by Magnetic Particles. First, nanofibers were decorated by magnetic nanoparticles through in situ precipitation of inorganic nanoparticles on NFC nanofibers, see the left section of Figure 1. The procedure involves precipitation of precursor particles, which are converted to magnetic nanoparticles during 3 h at 90 °C.[34,38] The successful decoration of NFC nanofibers by 42 nm (measured average diameter) large magnetic nanoparticles was confirmed by TEM, see Figure 2. The absence of observable individual particles or particle clusters suggested that the particles were firmly bonded to cellulose nanofibers, in a similar fashion as reported in previous studies on this system.[34,38] The inorganic content constituted 96.5 wt % of the 10 nm wide cellulose nanofibrils[32,33] as determined by thermogravimetrical analysis. Figures 2a and b also display occasionally observed acicular rods of metal oxo-hydroxide phase. This phase constituted a negligible volume fraction of the total inorganic phase (confirmed by magnetic measurements) and was present as remains from intermediate stages of the conversion from metal ions to ferrite during aqueous precipitation.[34] On average, one $CoFe_2O_4$ nanoparticle was attached for every 70 nm along the decorated 1−5 μm NFC, and the particle size distribution is also provided (Figure 2c and d). The structure of the NFC network with magnetic nanoparticles is also illustrated in Figure 2d. In Figure 2b, a qualitative impression of nanofiber size distribution as well as the presence of nanoparticle-rich regions is presented.[31] The sections of nanofibers without nanoparticles may relate to regions of increased surface tension, which did not allow for grafting of the oxo-hydroxide precursor phase prior to the transformation into ferrite particles.[34]

Structure of High Inorganic Content Nanocomposites. Two types of nanocomposite materials were prepared, see Figure 1. In the first type, decorated NFC nanofibers were combined with neat NFC to prepare porous nanofiber network composites with magnetic nanoparticles. A papermaking filtering approach was used to prepare a wet nanofiber "mat". This was predried and then subjected to compression molding to form stiff and strong solid composites with some porosity (28−36%). This material is essentially magnetic nanoparticles in a porous NFC nanofiber matrix ($CoFe_2O_4$/NFC). The volume fraction of $CoFe_2O_4$ was determined by the amount of neat NFC added and the final porosity. The second type of nanocomposite was prepared by impregnation of the compression molded $CoFe_2O_4$/NFC by epoxy (EP), see Figure 1. This material consists of magnetic nanoparticles in a matrix of NFC and EP (termed $CoFe_2O_4$/NFC/EP). Typical porosities of this second type of nanocomposite is in the 4−7% range, see Table 1.

Table 1. Summary of the Composition of the Final Materials

sample name	$CoFe_2O_4$[a] (wt %)	NFC[a] (wt %)	epoxy[a] (wt %)	porosity[b] (vol %)	density[b] (g/cm^3)
$CoFe_2O_4$-77/NFC	77	23	0	28	2.3
$CoFe_2O_4$-83/NFC	83	17	0	28	2.5
$CoFe_2O_4$-89/NFC	89	11	0	34	2.5
$CoFe_2O_4$-93/NFC	93	7	0	36	2.7
$CoFe_2O_4$-70/NFC/EP	70	20	10	5	2.5
$CoFe_2O_4$-76/NFC/EP	76	15	9	7	2.6
$CoFe_2O_4$-79/NFC/EP	79	12	9	4	2.9
$CoFe_2O_4$-84/NFC/EP	84	6	10	5	3.0

[a]Values from a single measurement, the experimental error is estimated at ±2%. [b]Values from a single measurement, the experimental error is estimated at ±5%.

Network Formation. A consequence of the high weight fraction of inorganics decorated onto the NFC nanofibers (96.5 wt % $CoFe_2O_4$) was that the filtered network had an insufficient amount of cellulose-cellulose connecting points. As a consequence, the mechanical properties were not good enough. Neat NFC (in different amounts) was therefore mixed with the decorated NFC prior to filtration and compression-molding (see Figure 1) to ascertain the formation of a "complete" nanofiber network (illustrated in Figure 2d). This resulted in inorganic contents ($CoFe_2O_4$) ranging from 77 to 93 wt %, see Table 1. Figures 3 a−c show the microstructure of the fractured $CoFe_2O_4$-93/NFC composite (containing 93 wt % ferrite) post compression. A homogeneous distribution of nanoparticles throughout the material was apparent for all contents of ferrite. The uniform inorganic phase distribution originated from the separation of the decorated nanofibers in their suspended state (along the fibrils). The colloidal processing route in Figure 1 allowed the formation of a network material as the decorated NFC was combined with neat NFC (Figure 2d). A characteristic of the composites was the typical stratified structure (Figure 3a) from the filtration process, which gives the network a strong two-dimensional character. The NFC tended to be aligned in-plane within the molded sheet structures. The evenly blended neat NFC was completely miscible with the modified nanofibers, and aggregates were not apparent in fracture surfaces.

Network Impregnation. In Figures 3b and c, it is apparent that voids are present between the nanoparticles in the $CoFe_2O_4$-93/NFC composite. The porosity accounted for 36 vol % of this materials, despite the high pressure (50 MPa) used during compression-molding and drying. The void space was continuous so that epoxy resin impregnation was possible, see Figure 1 and the Experimental Section. After resin impregnation, the porosity decreased to 5 vol %. Figures 3 d−f show the corresponding $CoFe_2O_4$-84/NFC/EP nanocomposites, display-

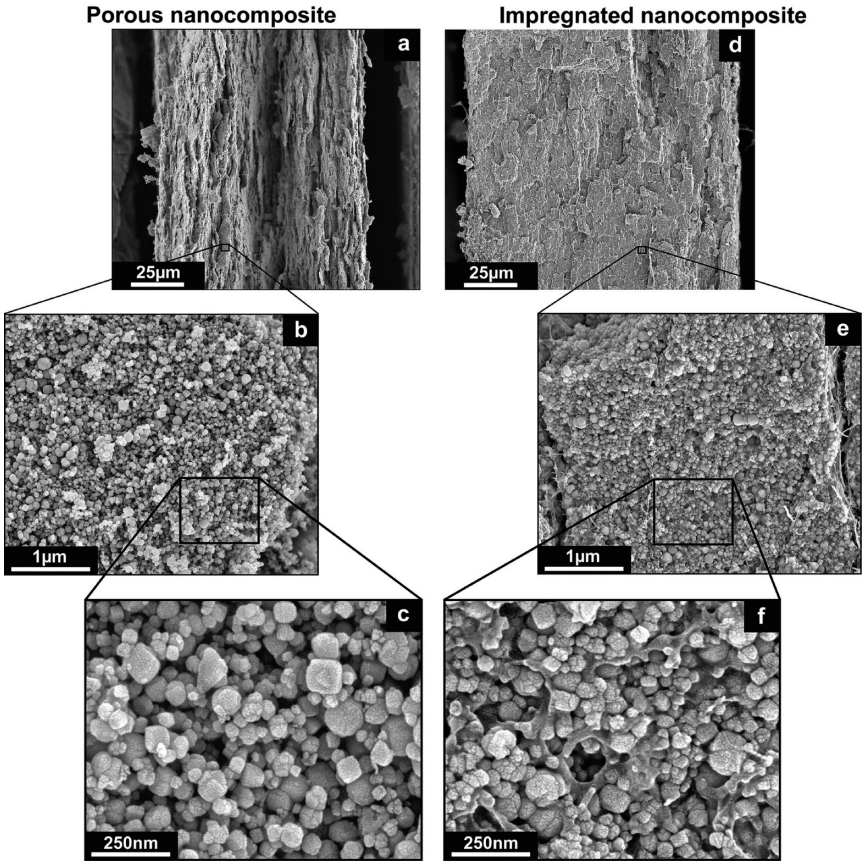

Figure 3. Scanning electron micrographs of fracture surfaces for $CoFe_2O_4$-93/NFC porous nanocomposites with 51 vol % $CoFe_2O_4$ (**a**–**c**) and impregnated $CoFe_2O_4$-84/NFC/EP nanocomposites with 53 vol % $CoFe_2O_4$ (**d**–**f**).

Table 2. Mechanical Property Data with the Calculated Volume Fractions of Each Component–Standard Deviation in Brackets

sample name	$CoFe_2O_4$[a] (vol %)	NFC[a] (vol %)	epoxy[a] (vol %)	porosity[b] (vol %)	E[c] (GPa)	σ[d] (MPa)
$CoFe_2O_4$-77/NFC	36	36	0	28	7.0 *(0.2)*	64 *(3)*
$CoFe_2O_4$-83/NFC	43	29	0	28	7.5 *(0.1)*	43 *(1)*
$CoFe_2O_4$-89/NFC	46	20	0	34	7.1 *(0.5)*	11 *(1)*
$CoFe_2O_4$-93/NFC	51	13	0	36	7.1 *(1.1)*	11 *(1)*
$CoFe_2O_4$-70/NFC/EP	36	36	23	5	12.6 *(0.1)*	97 *(6)*
$CoFe_2O_4$-76/NFC/EP	42	28	23	7	11.5 *(0.4)*	60 *(1)*
$CoFe_2O_4$-79/NFC/EP	48	24	24	4	14.7 *(0.3)*	45 (5)
$CoFe_2O_4$-84/NFC/EP	53	13	29	5	16.8 *(0.7)*	35 *(6)*

[a]Values from a single measurement, the experimental error is estimated at ±2%. [b]Values from a single measurement, the experimental error is estimated at ±5%. [c]E, Young's modulus. [d]σ, ultimate tensile strength.

ing a smooth fracture surface as compared to $CoFe_2O_4$-93/NFC (Figures 3a–c). The nanocomposite with an NFC/EP matrix showed a structure with a homogeneous distribution of up to 81 wt % magnetic nanoparticles. This is to our best knowledge the highest reported for magnetic nanoparticle contents in a thermosetting matrix. This is an achievement in strong contrast to the commonly observed agglomeration tendencies of magnetic nanoparticles in nanocomposites.[39]

Mechanical Properties. *Cellulose Network Response to Deformation.* Stress–strain curves in tension and mechanical property data are presented in Tables 1 and 2 and in Figure 4. The $CoFe_2O_4$-93/NFC with 36 vol % $CoFe_2O_4$ exhibits substantial ductility (5.4% strain to failure) and an ultimate strength of 64 MPa. The strain to failure (above 5%) is approaching that of neat NFC nanopaper (6–7%).[40] This indicates that the NFC preserves its cohesive network characteristics to high strains even at fairly high inorganic content. The failure mechanisms thus appear to be more favorable compared with polymer matrix composites. For the $CoFe_2O_4$/NFC nanocomposites, increased inorganic particle content resulted in substantially decreased strength (Figure 5b) and ductility (Figure 4), the reason is that the NFC network carries the major load. As the NFC content was reduced to 20 and 11 vol %, with increased porosity, the tensile strength was reduced to only 11 MPa, see Table 2. The Young's modulus values for $CoFe_2O_4$/NFC were in the range 6–8 GPa for all compositions. It contrasts with the behavior observed at lower particle contents in a previous study,[34] where a linear decrease in modulus was observed with increasing nanoparticle content due to NFC network disruption. A possible explanation is that the $CoFe_2O_4$ nanoparticles provide some contribution to modulus in the present compression molded material. This and

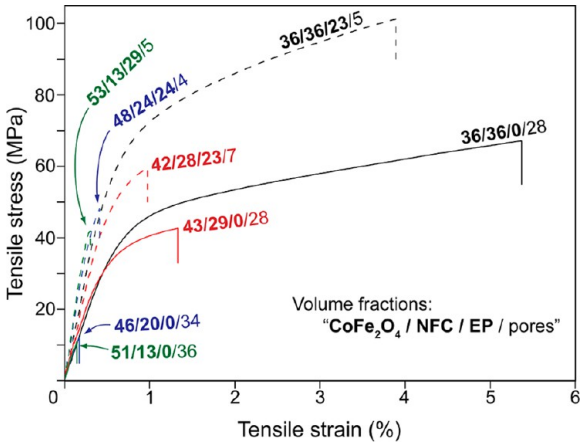

Figure 4. Tensile stress strain curves for the porous (continuous lines) and impregnated (dashed lines) nanocomposites with different nanoparticle contents.

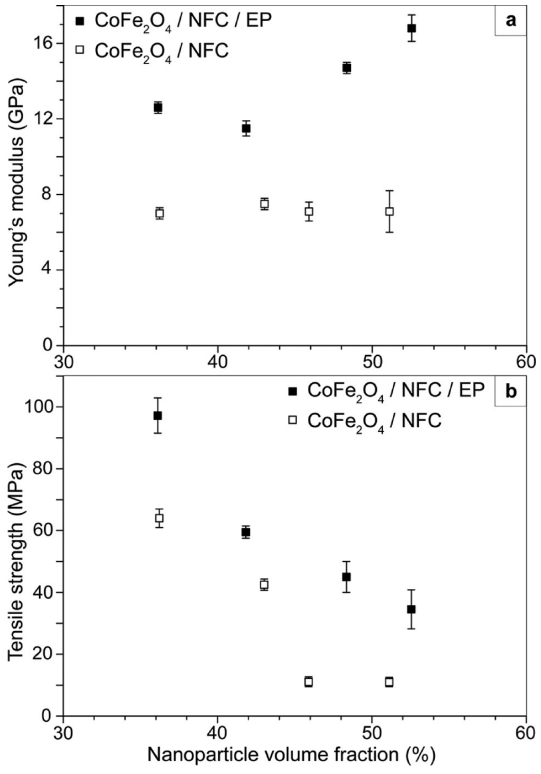

Figure 5. Young's modulus (**a**) and tensile strength (**b**) as a function of volume fraction of $CoFe_2O_4$ nanoparticles for porous (empty squares) and impregnated (filled squares) nanocomposites.

a slight porosity increase explain why modulus is virtually unchanged as NFC content is reduced and $CoFe_2O_4$ content is increased. The Young's modulus of spinel ferrite nanoparticles is ca. 100−120 GPa.[41]

Effect of Epoxy Impregnation. Impregnation of the porous material with epoxy resulted in increased tensile strength; from 64 to 97 MPa at the lowest nanoparticle content (36 vol %) and from 11 to 35 MPa for the highest content (53 vol %), see Figure 4. The polymer matrix simply improves stress transfer in the composite structure. The toughness (area under stress−strain curve) increased for most compositions, see Figure 4, with the largest improvements for the highest nanoparticle contents. Even though the inorganic particle content is high (>70 wt % or 36−53 vol %), the NFC network combined with epoxy provided considerable ductility, especially for the composition with 36 vol % NFC.

Young's modulus is plotted against nanoparticle volume fraction in Figure 5a. Epoxy impregnation resulted in an improved modulus from around 7 GPa to the range 11.6−16.8 GPa, Figure 5a. The highest relative increase in modulus is for the highest nanoparticle content. Apparently, the epoxy matrix is critical for favorable stress transfer and bonds the NFC/EP polymer matrix to the stiff cobalt ferrite particles.

In Figure 5b, tensile strength versus nanoparticle content is presented with and without epoxy matrix. In both cases, strength decreases with particle volume fraction. The classical explanation for stiff particle composites is that higher particle content leads to increased strain concentration, so that debond cracks form at lower strain.[42] In the present case, the explanation may be more complicated since NFC content is decreased with increased nanoparticle content.

Magnetic Properties. Magnetization hysteresis curves for NFC/nanoparticle composites are presented in Figure 6a. The wide hysteresis is characteristic of the hard magnetic behavior of $CoFe_2O_4$, with a coercivity of 99 ± 1 kA/m (see Table 3) independent of nanoparticle content. For the present range of magnetic particle content the magnetization is proportional and the coercivity is essentially unaffected. This is consistent with that the magnetic properties of the nanocomposite is due to a simple summation of the individual particle's contribution. Despite the apparently rather closely packed nanoparticles (see Figure 3) there is negligible effect on the magnetic properties. This is in contrast to other systems where magnetic particle−particle interactions can have complex effects on e.g. coercivity.[43]

The magnetization values showed a linear increase (Figure 6a inset) in remanent and saturation magnetization as a function of nanoparticle content, up to 40 and 68 $A{\cdot}m^2/kg$, respectively. At a given weight fraction of magnetic material, the impregnation with epoxy resin did not show any detectable effect on the magnetic properties.

The magnetization value normalized to the particle mass were typical for this type of nanoparticles (ca. 70 $A{\cdot}m^2/kg$) and comparable to previously reported data.[34] Therefore, the presence of residual nonferrite phase (see Figure 2b) did not affect magnetic properties. This suggests that the nonferrite phase is of very low volume fraction.

All nanocomposite samples were able to sustain their own weight after magnetization when in contact with a non-magnetized ferromagnetic surface (e.g., steel, see Figure 6b). The reasons include high magnetic nanoparticle content and high coercivity. This demonstrates the potential magnetic strength in these permanent nanocomposite magnets, especially in relation to their relatively low density.

Thermal Stability. TGA curves showing the thermal stability of the materials are presented in Figure 7. An initial weight loss was observed up to 120 °C corresponding to water release from the hygroscopic cellulose composites. The residual mass at 120 °C was therefore taken as reference mass for completely dry materials. The degradation temperatures of porous $CoFe_2O_4$-93/NFC nanocomposites were in the range 220−230 °C. This is significantly lower than for the neat NFC nanopaper, which degraded at ca. 300 °C.[34] The reason is that oxidative degradation of polysaccharides[44] and other polymers (e.g., poly(ethylene oxide)[45]) is accelerated in the presence of metal oxide compounds. In particular, oxidative degradation of

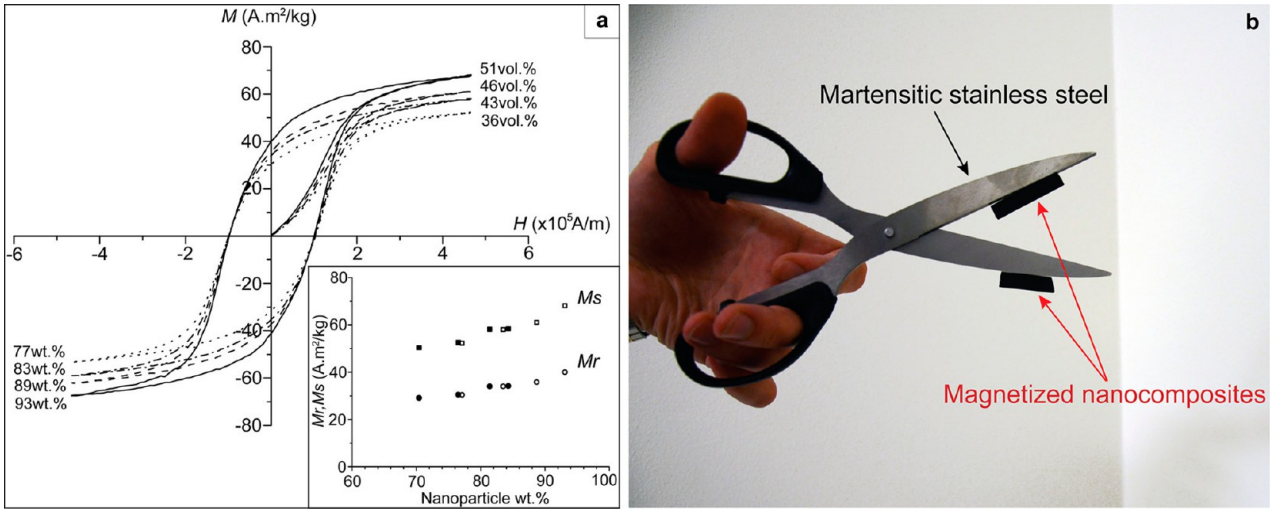

Figure 6. **a**: Hysteresis curves for porous nanocomposites with different nanoparticle contents (indicated on graph in vol % and wt %); inset: remanent and saturation magnetization as a function of nanoparticle content (empty squares: porous; filled squares: impregnated nanocomposite); **b**: picture showing permanent magnetic nanocomposite sheets holding their own weight when put in contact with a steel surface (epoxy-impregnated with 76 wt % $CoFe_2O_4$).

Table 3. Magnetic Data for Each Composite Material Composition

sample name	Mr[a] (A·m²/kg)	Ms[b] (A·m²/kg)	coercivity (kA/m)	susceptibility (10^{-3} m³/kg)
$CoFe_2O_4$-77/NFC	30.4	52.3	99.4	0.15
$CoFe_2O_4$-83/NFC	34.0	58.0	99.6	0.13
$CoFe_2O_4$-89/NFC	35.8	61.0	99.1	0.16
$CoFe_2O_4$-93/NFC	40.0	68.1	98.0	0.17
$CoFe_2O_4$-70/NFC/EP	29.1	50.4	99.3	0.13
$CoFe_2O_4$-76/NFC/EP	30.5	52.6	98.4	0.14
$CoFe_2O_4$-79/NFC/EP	34.0	58.1	98.1	0.15
$CoFe_2O_4$-84/NFC/EP	34.2	58.4	98.1	0.16

[a]Mr, remanent magnetization. [b]Ms, saturation magnetization.

paper is catalyzed by iron and cobalt compounds.[46] However, this decrease in degradation temperature was not observed in the nanocomposites with lower nanoparticle content (up to 60 wt %).[34] The long-term thermal stability of the material with the higher amount of nanoparticle content was therefore evaluated under an isothermal heating at 120 °C. The material did not show any degradation and a weight loss of only 0.08% after 5 h (oxygen), which ascertained that the modified fibers could be used in extensive curing cycles with a thermoset.

Impregnation with EP increased the degradation temperature of the nanocomposites to around 300 °C. Apparently, the epoxy matrix (degradation temperature: ca. 400 °C) provided some protection for the decorated cellulose fibrils. A tentative explanation is that decreased oxygen permeability improves cellulose stability against oxidative degradation.

The thermomechanical properties were studied by DMTA analysis. Results for samples with initial nanoparticle content

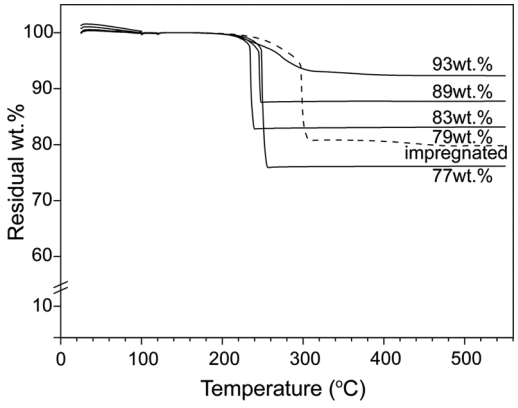

Figure 7. TGA curves for the degradation in O_2 of the porous hybrid/NFC nanocomposites with different inorganic content (continuous lines) and one of the EP impregnated compositions (dashed line).

(before impregnation) of 89 wt % are reported in Figure 8. The nonimpregnated porous NFC/nanoparticle composite did not

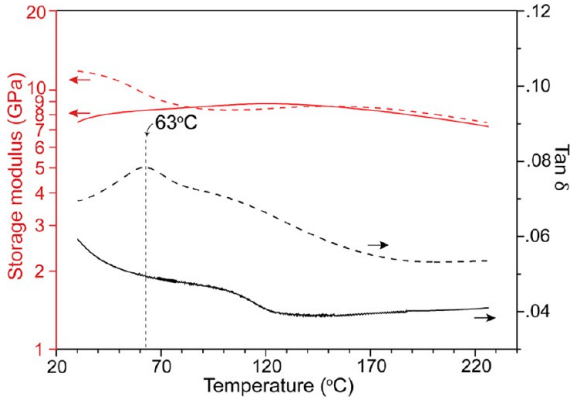

Figure 8. Storage modulus and tan(δ) curves from DMTA analysis of the porous (continuous lines) and impregnated (dashed lines) nanocomposites with initial nanoparticle content of 89 wt % (after impregnation 79 wt %).

dx.doi.org/10.1021/am506134k | ACS Appl. Mater. Interfaces 2014, 6, 20524−20534

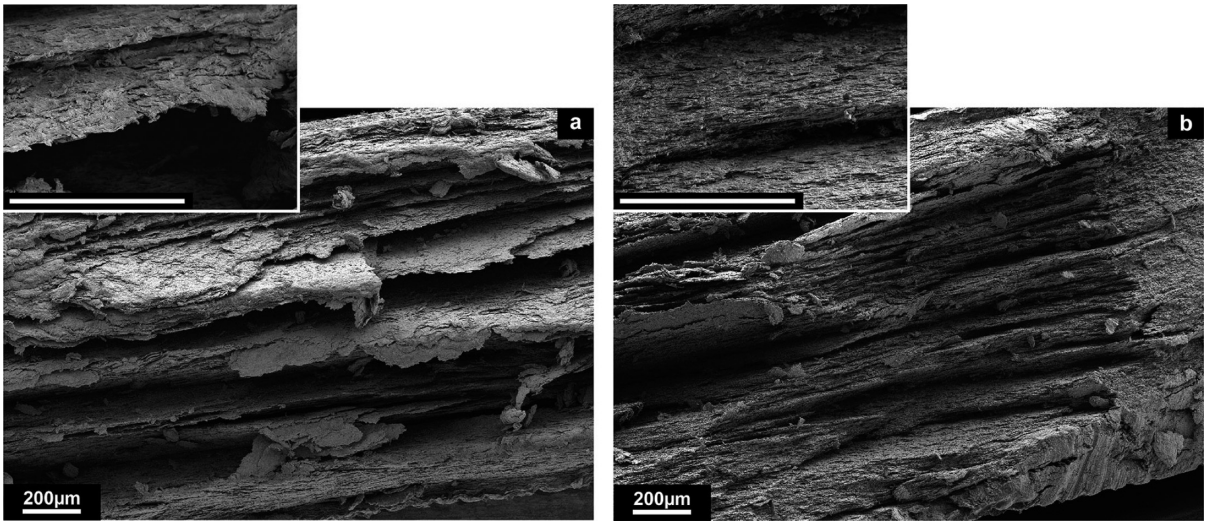

Figure 9. Scanning electron micrographs of fracture surface cross sections for the multilayer nanocomposites with and without epoxy-impregnation: (a) $CoFe_2O_4$-83/NFC with 41 vol % $CoFe_2O_4$ and 30% porosity (b) $CoFe_2O_4$-76/NFC/EP with 42 vol % $CoFe_2O_4$ and 7% porosity. Scale bars are 200 μm in length.

soften up to the decomposition temperature (220 °C). The storage modulus was maintained at around 8−9 GPa, due to the stiff cellulose nanofibril network and the high thermo-mechanical stability of the crystalline cellulose nanofibrils.[47] The transition observed on the tan δ plot around 100 °C can be explained by evaporation of adsorbed water at fibrils and particles surface. In the presence of the epoxy matrix, the composites exhibit a glass transition at 63 °C, corresponding to the epoxy matrix as demonstrated by the characteristic peak in tan δ (Figure 8). Across the glass transition, the storage modulus decreased only from 11 to 8 GPa. The high storage modulus at the rubbery plateau can be explained by the high content of thermally stable inclusions (in total 70 vol % of NFC + nanoparticles). Cellulose nanofibril networks have been reported to act as a very efficient reinforcement in the rubbery region due to the formation of a percolating network, even at low volume fractions.[48−50]

Multilayer Nanocomposite Plates. The feasibility of compression molding was further demonstrated. Ten layers of wet sheets were stacked on top of each other directly after filtration. The sheets were based on a mixture of NFC fibrils decorated by $CoFe_2O_4$ nanoparticles and additional neat NFC fibrils for the purpose of better mechanical properties of the network. Drying under compression resulted in coalescence of the hybrid nanocomposite sheets to a low-porosity material, without the need for additional binder. Neat NFC fibrils apparently had a binding function. The materials with an initial $CoFe_2O_4$ content of 83 wt % were evaluated (41 vol % $CoFe_2O_4$ and 30% porosity). Also, the same multilayer porous substrate was impregnated by EP resin and cured to obtain a $CoFe_2O_4$ content of 76 wt % (42 vol % $CoFe_2O_4$ and 7% porosity).

These materials combine magnetic functionality, mechanical properties, and large-scale industrial processability. The morphology of fracture surfaces after flexural tests are presented in Figure 9. On a micrometer scale, a layered structure is apparent. Note that the thickness of fractured layers is smaller than the thickness of the 10 stacked layers (120−150 μm). The nonimpregnated composite showed delamination cracking between the thin layers (Figure 9a). In contrast, the EP impregnated and less porous material showed a much lower extent of delamination cracking and a more even fracture surface (Figure 9b).

This indicates improved delamination strength between layers due to the EP matrix and the lower porosity. The processing route relies on preparation of a dry nanoporous network prior to impregnation and in combination with the decorated NFC this results in homogeneous nanoparticle distribution (absence of epoxy-rich regions between layers).

The nanocomposite plates were tested in three-point bending, and the stress−strain curves are presented in Figure 10. The high flexural strength (60 MPa) for the non-

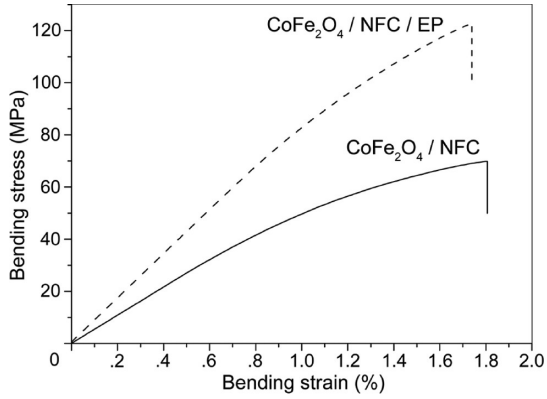

Figure 10. Estimated stress−strain curves from load-deflection curves in flexural tests of porous (continuous line) and EP-impregnated (dashed line) multilayer nanocomposite plates. The porosity of $CoFe_2O_4$-83/NFC is about 30%, whereas impregnated $CoFe_2O_4$-76/NFC/EP has 7% porosity.

impregnated multilayer nanocomposite confirms good adhesion between sheets of hybrid NFC networks without the help of any additional binder. Intimate NFC-NFC contact due to capillary forces during drying results in strong secondary interactions between these layers (classical paper-forming mechanism).

Impregnation with the epoxy resin doubled the flexural strength (120 MPa). The EP resin improves stress-transfer in the hybrid NFC/nanoparticle network (see data in Table 2 for

single layer sheets); the EP matrix also reduces porosity from 30 to 7% and increases delamination strength. The multiscale material organization allows load-transfer throughout the millimeter-thick nanostructured composite despite very high nanoparticle content.

More complex objects can be obtained by using a mold with desired shape. The process never involves temperature above 120 °C, which contrasts with traditional ferrite magnets processing requiring sintering temperatures of several hundreds to thousands of degrees Celsius.[51] As a demonstration we prepared multilayer 1.2 mm-thick nanocomposite permanent magnets with 3D shape (half-ring), as presented in Figure 11. Thus, complex macroscopic magnetic components can be readily fabricated based on nanoparticle decorated cellulose nanofibers through conventional compression molding.

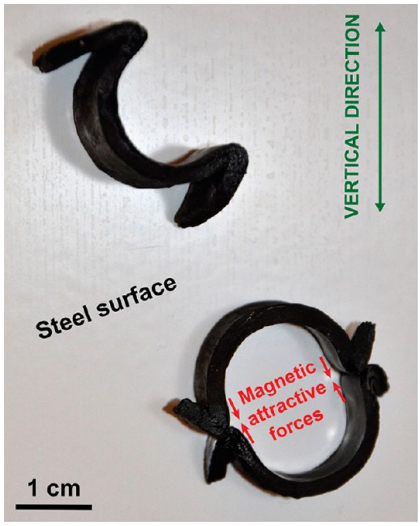

Figure 11. Image of multilayer nanocomposite permanent magnets supporting their own weight against a nonmagnetized steel surface (a refrigerator door).

CONCLUSIONS

Homogeneous magnetic nanocomposites with high nanoparticle content (77−93 wt % $CoFe_2O_4$) were successfully prepared by filtration of a hydrocolloidal suspension of decorated cellulose nanofibrils obtained from dilution of 96.5 wt % "master-batch" of functional fibers, followed by compression molding. As-obtained nanocomposite sheets consisted of a porous hybrid NFC/nanoparticle network with uniform distribution of nanoparticles. The inherent porosity allowed for impregnation with an epoxy resin (EP). This increased the modulus from around 7 GPa to 13−17 GPa, depending on ferrite content. For the highest ferrite contents (89−93 wt %, i.e. 46−51 vol %), the tensile strengths were significantly increased (>3 times higher) by the EP impregnation. The reason for these improvements was that the continuous EP matrix provided better stress distribution, so that the cellulose nanofibers and the ferrite particles carried higher stress. When the cellulose nanofiber content was 36 vol %, the material also demonstrated considerable ductility and toughness, even though the ferrite content was as high as 77 wt % (36 vol %). Furthermore, an improved thermal stability was also observed for the EP impregnated nanocomposites.

As the magnetic nanoparticle content was increased from 77 to 93 wt %, the remanent and saturation magnetization increased proportionally from 30 to 34 and 52 to 68 $A{\cdot}m^2/kg$, respectively, whereas the corcivity (99 kA/m) remained unaffected. The nanocomposites could therefore be regarded as a permanent magnetic materials, where the magnetic properties from the Co-ferrite nanoparticles were retained.

The successful preparation of millimeter-thick multilayer nanocomposite plates demonstrates the advantageous combination of magnetic and thermomechanical properties, which has the potential to be realized also at a larger scale. The development of the presented "master-batch" approach could thus enable the production of magnetic nanocomposites of high functionality, by the use of native cellulose and a low temperature (<120 °C) molding process.

AUTHOR INFORMATION

Corresponding Authors

*Phone: 46 73 2701868. Fax: 46 8 7906036. E-mail: rols@kth.se.

*Phone: 46 8 7908118. Fax: 46 8 207865. E-mail: blund@kth.se.

Present Address

[‖]Ecole Polytechnique Fédérale de Lausanne (EPFL) − STI − IMX − LMOM, MXG 037, Station 12−1015 Lausanne, Switzerland.

Author Contributions

The manuscript was written through contributions of all authors. All authors have given approval to the final version of the manuscript. S.G. wrote the paper and performed the experiments. R.L.A., V.S., R.T.O., and L.A.B. reviewed and edited the manuscript. R.L.A. helped with electron microscopy. V.S. contributed to the magnetic characterization and interpretation of results. R.T.O. and L.A.B. supervised this research project.

Notes

The authors declare no competing financial interest.

ACKNOWLEDGMENTS

The Knut and Alice Wallenberg Foundation is acknowledged for its financial support to the Wallenberg Wood Science Center (WWSC). We would like to thank Dr. Michaela Salajková for her help with TEM imaging.

REFERENCES

(1) Burda, C.; Chen, X.; Narayanan, R.; El-Sayed, M. A. Chemistry and Properties of Nanocrystals of Different Shapes. *Chem. Rev.* **2005**, *105*, 1025−1102.

(2) Klimov, V. I. *Semiconductor and Metal Nanocrystals: Synthesis and Electronic and Optical Properties*; 2004.

(3) Gubin, S. P. *Magnetic Nanoparticles*; John Wiley & Sons: 2009.

(4) Sanchez, C.; Belleville, P.; Popall, M.; Nicole, L. Applications of Advanced Hybrid Organic-Inorganic Nanomaterials: From Laboratory to Market. *Chem. Soc. Rev.* **2011**, *40*, 696−753.

(5) Balazs, A. C.; Emrick, T.; Russell, T. P. Nanoparticle Polymer Composites: Where Two Small Worlds Meet. *Science* **2006**, *314*, 1107−1110.

(6) Zou, H.; Wu, S.; Shen, J. Polymer/Silica Nanocomposites: Preparation, Characterization, Properties, and Applications. *Chem. Rev.* **2008**, *108*, 3893−3957.

(7) O'Regan, B.; Grätzel, M. A Low-Cost, High-Efficiency Solar Cell Based on Dye-Sensitized Colloidal TiO2 Films. *Nature* **1991**, *353*, 737−740.

(8) Stankovich, S.; Dikin, D. A.; Dommett, G. H. B.; Kohlhaas, K. M.; Zimney, E. J.; Stach, E. A.; Piner, R. D.; Nguyen, S. T.; Ruoff, R. S. Graphene-Based Composite Materials. *Nature* **2006**, *442*, 282−286.
(9) Usuki, A.; Hasegawa, N.; Kato, M.; Kobayashi, S. Polymer-Clay Nanocomposites. *Adv. Polym. Sci.* **2005**, *179*, 135−195.
(10) Dai, Q.; Nelson, A. Magnetically-Responsive Self Assembled Composites. *Chem. Soc. Rev.* **2010**, *39*, 4057−4066.
(11) Behrens, S. Preparation of Functional Magnetic Nanocomposites and Hybrid Materials: Recent Progress and Future Directions. *Nanoscale* **2011**, *3*, 877−892.
(12) Zhang, H.; Han, J.; Yang, B. Structural Fabrication and Functional Modulation of Nanoparticle−Polymer Composites. *Adv. Funct. Mater.* **2010**, *20*, 1533−1550.
(13) Rafiee, M. A.; Rafiee, J.; Wang, Z.; Song, H.; Yu, Z.-Z.; Koratkar, N. Enhanced Mechanical Properties of Nanocomposites at Low Graphene Content. *ACS Nano* **2009**, *3*, 3884−3890.
(14) Lee, S.; Hong, J.-Y.; Jang, J. The Effect of Graphene Nanofiller on the Crystallization Behavior and Mechanical Properties of Poly(vinyl alcohol). *Polym. Int.* **2012**, *6*, 901−908.
(15) Xu, W.; Raychowdhury, S.; Jiang, D. D.; Retsos, H.; Giannelis, E. P. Dramatic Improvements in Toughness in Poly(lactide-co-glycolide) Nanocomposites. *Small* **2008**, *4*, 662−669.
(16) Xiong, H.-M. Photoluminescent ZnO Nanoparticles Modified by Polymers. *J. Mater. Chem.* **2010**, *20*, 4251−4262.
(17) Zhou, T. H.; Ruan, W. H.; Rong, M. Z.; Zhang, M. Q.; Mai, Y. L. Keys to Toughening of Non-layered Nanoparticles/Polymer Composites. *Adv. Mater.* **2007**, *19*, 2667−2671.
(18) Mammeri, F.; Bourhis, E. L.; Rozes, L.; Sanchez, C. Mechanical Properties of Hybrid Organic-Inorganic Materials. *J. Mater. Chem.* **2005**, *15*, 3787−3811.
(19) Cheng, D. F.; Hozumi, A. Highly Loaded Silicone Nanocomposite Exhibiting Quick Thermoresponsive Optical Behavior. *ACS Appl. Mater. Interfaces* **2011**, *3*, 2219−2223.
(20) Wang, Y.; Wu, X.; Yang, W.; Zhai, Y.; Xie, B.; Yang, M. Aggregate of Nanoparticles: Rheological and Mechanical Properties. *Nanoscale Res. Lett.* **2011**, *6*, 114.
(21) Bomal, Y.; Godard, P. Melt Viscosity of Calcium-Carbonate-Filled Low Density Polyethylene: Influence of Matrix-Filler and Particle-Particle Interactions. *Polym. Eng. Sci.* **1996**, *36*, 237−243.
(22) Guo, Z.; Park, S.; Wei, S.; Pereira, T.; Moldovan, M.; Karki, A. B.; Young, D. P.; Hahn, H. T. Flexible High-Loading Particle-Reinforced Polyurethane Magnetic Nanocomposite Fabrication Through Particle-Surface-Initiated Polymerization. *Nanotechnology* **2007**, *18*, 335704.
(23) Walther, A.; Bjurhager, I.; Malho, J.-M.; Pere, J.; Ruokolainen, J.; Berglund, L. A.; Ikkala, O. Large-Area, Lightweight and Thick Biomimetic Composites with Superior Material Properties via Fast, Economic, and Green Pathways. *Nano Lett.* **2010**, *10*, 2742−2748.
(24) Yao, H.-B.; Guan, Y.; Mao, L.-B.; Wang, Y.; Wang, X.-H.; Tao, D.-Q.; Yu, S.-H. A Designed Multiscale Hierarchical Assembly Process to Produce Artificial Nacre-Like Freestanding Hybrid Films with Tunable Optical Properties. *J. Mater. Chem.* **2012**, *22*, 13005−13012.
(25) Zhu, W.; Lu, C.-H.; Chang, F.-C.; Kuo, S.-W. Supramolecular Ionic Strength-Modulating Microstructures and Properties of Nacre-Like Biomimetic Nanocomposites Containing High Loading Clay. *RSC Adv.* **2012**, *2*, 6295−6305.
(26) Podsiadlo, P.; Kaushik, A. K.; Arruda, E. M.; Waas, A. M.; Shim, B. S.; Xu, J.; Nandivada, H.; Pumplin, B. G.; Lahann, J.; Ramamoorthy, A.; Kotov, N. A. Ultrastrong and Stiff Layered Polymer Nanocomposites. *Science* **2007**, *318*, 80−83.
(27) McClure, S. A.; Worfolk, B. J.; Rider, D. A.; Tucker, R. T.; Fordyce, J. A. M.; Fleischauer, M. D.; Harris, K. D.; Brett, M. J.; Buriak, J. M. Electrostatic Layer-by-Layer Assembly of CdSe Nanorod/Polymer Nanocomposite Thin Films. *ACS Appl. Mater. Interfaces* **2009**, *2*, 219−229.
(28) Zhu, J.; Wei, S.; Ryu, J.; Sun, L.; Luo, Z.; Guo, Z. Magnetic Epoxy Resin Nanocomposites Reinforced with Core−Shell Structured Fe@FeO Nanoparticles: Fabrication and Property Analysis. *ACS Appl. Mater. Interfaces* **2010**, *2*, 2100−2107.
(29) He, Q.; Yuan, T.; Zhu, J.; Luo, Z.; Haldolaarachchige, N.; Sun, L.; Khasanov, A.; Li, Y.; Young, D. P.; Wei, S.; Guo, Z. Magnetic High Density Polyethylene Nanocomposites Reinforced with In-situ Synthesized Fe@FeO Core-Shell Nanoparticles. *Polymer* **2012**, *53*, 3642−3652.
(30) Guo, Z.; Lei, K.; Li, Y.; Ng, H. W.; Prikhodko, S.; Hahn, H. T. Fabrication and Characterization of Iron Oxide Nanoparticles Reinforced Vinyl-Ester Resin Nanocomposites. Compos. *Sci. Technol.* **2008**, *68*, 1513−1520.
(31) Henriksson, M.; Henriksson, G.; Berglund, L. A.; Lindström, T. An Environmentally Friendly Method for Enzyme-Assisted Preparation of Microfibrillated Cellulose (MFC) Nanofibers. *Eur. Polym. J.* **2007**, *43*, 3434−3441.
(32) Sehaqui, H.; Zhou, Q.; Berglund, L. A. High-Porosity Aerogels of High Specific Surface Area Prepared From Nanofibrillated Cellulose (NFC). *Compos. Sci. Technol.* **2011**, *71*, 1593−1599.
(33) Sacui, I. A.; Nieuwendaal, R. C.; Burnett, D. J.; Stranick, S. J.; Jorfi, M.; Weder, C.; Foster, E. J.; Olsson, R. T.; Gilman, J. W. Comparison of the Properties of Cellulose Nanocrystals and Cellulose Nanofibrils Isolated from Bacteria, Tunicate, and Wood Processed Using Acid, Enzymatic, Mechanical, and Oxidative Methods. *ACS Appl. Mater. Interfaces* **2014**, *6*, 6127−6138.
(34) Galland, S.; Andersson, R. L.; Salajková, M.; Ström, V.; Olsson, R. T.; Berglund, L. A. Cellulose Nanofibers Decorated with Magnetic Nanoparticles − Synthesis, Structure and Use in Magnetized High Toughness Membranes for a Prototype Loudspeaker. *J. Mater. Chem. C* **2013**, *1*, 7963−7972.
(35) Ansari, F.; Galland, S.; Johansson, M.; Plummer, C. J. G.; Berglund, L. A. Cellulose Nanofiber Network for Moisture Stable, Strong and Ductile Biocomposites and Increased Epoxy Curing Rate. *Composites, Part A* **2014**, *63*, 35−44.
(36) Olsson, R. T.; Salazar-Alvarez, G.; Hedenqvist, M. S.; Gedde, U. W.; Lindberg, F.; Savage, S. J. Controlled Synthesis of Near-Stoichiometric Cobalt Ferrite Nanoparticles. *Chem. Mater.* **2005**, *17*, 5109−5118.
(37) Sun, C. C. True Density of Microcrystalline Cellulose. *J. Pharm. Sci.* **2005**, *94*, 2132−2134.
(38) Olsson, R. T.; Azizi Samir, M. A. S.; Salazar-Alvarez, G.; Belova, L.; Ström, V.; Berglund, L. A.; Ikkala, O.; Nogués, J.; Gedde, U. W. Making Flexible Magnetic Aerogels and Stiff Magnetic Nanopaper Using Cellulose Nanofibrils as Templates. *Nat. Nanotechnol.* **2010**, *5*, 584−588.
(39) Lalatonne, Y.; Richardi, J.; Pileni, M. P. Van der Waals versus Dipolar Forces Controlling Mesoscopic Organizations of Magnetic Nanocrystals. *Nat. Mater.* **2004**, *3*, 121−125.
(40) Henriksson, M.; Berglund, L. A.; Isaksson, P.; Lindström, T.; Nishino, T. Cellulose Nanopaper Structures of High Toughness. *Biomacromolecules* **2008**, *9*, 1579−1585.
(41) Kester, E.; Rabe, U.; Presmanes, L.; Tailhades, P.; Arnold, W. Measurement of Young's Modulus of Nanocrystalline Ferrites with Spinel Structures by Atomic Force Acoustic Microscopy. *J. Phys. Chem. Solids* **2000**, *61*, 1275−1284.
(42) Sjögren, B. A.; Berglund, L. A. Failure Mechanisms in Polypropylene with Glass Beads. *Polym. Compos.* **1997**, *18*, 1−8.
(43) Majetich, S. A.; Sachan, M. Magnetostatic Interactions in Magnetic Nanoparticle Assemblies: Energy, Time and Length Scales. *J. Phys. D: Appl. Phys.* **2006**, *39*, R407−R422.
(44) Kolar, J. Mechanism of Autoxidative Degradation of Cellulose. *Restaurator* **1997**, *18*, 163−176.
(45) Kaczmarek, H.; Sionkowska, A.; Kaminska, A.; Kowalonek, J.; Swiatek, M.; Szalla, A. The Influence of Transition Metal Salts on Photo-Oxidative Degradation of Poly(ethylene oxide). *Polym. Degrad. Stab.* **2001**, *73*, 437−441.
(46) Malešič, J.; Kočar, D.; Balažic, F. A. Stabilization of Copper- and Iron-Containing Papers in Mildly Alkaline Environment. *Polym. Degrad. Stab.* **2012**, *97*, 118−123.
(47) Sehaqui, H.; Zhou, Q.; Berglund, L. A. Nanostructured Biocomposites of High Toughness - A Wood Cellulose Nanofiber

Network in Ductile Hydroxyethylcellulose Matrix. *Soft Matter* **2011**, *7*, 7342−7350.
(48) Iwatake, A.; Nogi, M.; Yano, H. Cellulose Nanofiber-Reinforced Polylactic Acid. *Compos. Sci. Technol.* **2008**, *68*, 2103−2106.
(49) Malainine, M. E.; Mahrouz, M.; Dufresne, A. Thermoplastic Nanocomposites Based on Cellulose Microfibrils from Opuntia Ficus-Indica Parenchyma Cell. *Compos. Sci. Technol.* **2005**, *65*, 1520−1526.
(50) Azizi Samir, M. A. S.; Alloin, F.; Paillet, M.; Dufresne, A. Tangling Effect in Fibrillated Cellulose Reinforced Nanocomposites. *Macromolecules* **2004**, *37*, 4313−4316.
(51) Smiya, S. *Handbook of Advanced Ceramics*; Academic Press: 2003.